Multiband superconductivity in Mo_8Ga_{41} driven by a site-selective mechanism

Anshu Sirohi,[1] Surabhi Saha,[2] Prakriti Neha,[3] Shekhar Das,[1] Satyabrata Patnaik,[3] Tanmoy Das,[2] and Goutam Sheet[1,*]

[1]*Department of Physical Sciences, Indian Institute of Science Education and Research (IISER) Mohali, Sector 81, S. A. S. Nagar, Manauli, PO 140306, India*

[2]*Department of Physics, Indian Institute of Science, Bangalore 560012, India*

[3]*School of Physical Sciences, Jawaharlal Nehru University, New Delhi, PO 110067, India*

(Received 3 October 2018; revised manuscript received 22 November 2018; published 6 February 2019)

The family of the endohedral gallide cluster compounds recently emerged as a new family of superconductors which is expected to host systems displaying unconventional physics. Mo_8Ga_{41} is an important member of this family which shows relatively large $T_c \sim 10$ K and has shown indications of strong electron-phonon coupling and multiband superconductivity. Here, through direct measurement of superconducting energy gap by scanning tunneling spectroscopy (STS), we demonstrate the existence of two distinct superconducting gaps of magnitude 0.85 and 1.6 meV, respectively, in Mo_8Ga_{41}. Both gaps are seen to be conventional in nature as they evolve systematically with temperature as per the predictions of BCS theory. Our band structure calculations reveal that only two specific Mo sites in a unit cell contribute to superconductivity where only d_{xz}/d_{yz} and $d_{x^2-y^2}$ orbitals have strong contributions. Our analysis indicates that the site-elective contribution governs the two-gap nature of superconductivity in Mo_8Ga_{41}.

DOI: 10.1103/PhysRevB.99.054503

The rule of Matthias for predicting new superconductors with higher critical temperatures (T_c) [1] that says a higher density of states at the Fermi energy (E_F) is expected to lead to a higher T_c is partly followed by the endohedral gallide cluster family of superconductors with lower valence electron counts. For higher electron counts, beyond Mo_8Ga_{41} that superconducts below $T_c \sim 10$ K [2], the architecture of the cluster packing starts playing a dominant role in deciding T_c and in this regime, the T_c goes down though DOS at E_F goes up. This competition makes the T_c of Mo_8Ga_{41} maximum in the family [3]. Based on clear understanding of the relationship of the superconducting properties with the structural and electronic properties of these compounds, new electron counting rules were developed in which it has been possible to predict new superconductors belonging to the family that have also been experimentally realized [3]. Like many other families of superconductors, the superconductivity in the gallium cluster family might also emerge through complex pairing mechanism and host unconventional physics. Indications of unconventional superconductivity has already been obtained on a number of compounds belonging to this family. For example, in case of superconducting $PuCoGa_5$ it was argued that, like in high T_c cuprates, antiferromagnetic fluctuations might lead to superconducting pairing [4–6].

Based on a number of experiments that were employed to study the superconducting phase of Mo_8Ga_{41}, it was shown that this compound manifests unusually high electron-phonon coupling leading to a large Δ/k_BT_c ratio and indication of multigap superconductivity was also found [7,8]. In this article, from direct measurement of the superconducting energy gap through scanning tunneling spectroscopy (STS), we show that Mo_8Ga_{41}, like MgB_2, is a two-gap superconductor [9–16]. Two distinct gap structures are clearly resolved in the quasiparticle energy spectra. From detailed temperature dependent experiments we conclude that both gaps are conventional in nature. Through the band structure calculations, we have also identified the bands responsible for the two respective gaps. Our magnetic field dependent STS experiments further suggest that the interband coupling is weak in Mo_8Ga_{41}, as in case of MgB_2 [9].

Compact samples of Mo_8Ga_{41} were synthesized through solid state reaction by mixing constituent elements Mo (99.999%) powder and Ga (99.999%) pieces in stoichiometric ratio in a quartz ampoule which was evacuated down to 10^{-4} mbar and heated to 850 °C and then cooled down very slowly. The samples appeared shiny gray and the formation of Mo_8Ga_{41} in single phase was confirmed by powder x-ray diffraction followed by Rietveld analysis. A superconducting transition at $T_c \sim 10$ K was found from both temperature dependent resistivity and magnetization experiments. The STM and STS experiments were carried out in an ultrahigh vacuum (UHV) cryostat working down to 300 mK (Unisoku system with RHK R9 controller). The STM is equipped with a UHV sample preparation chamber, where a few layers of the surface was first removed by mild sputtering in an argon environment prior to the STS experiments. This ensured that we probed the pristine surface of Mo_8Ga_{41}.

In Fig. 1(a) we show an STM topographic image showing distinctly visible grains with average grain size ∼5 nm. For spectroscopic measurements, we first brought the STM tip on the central parts of the grains and recorded the dI/dV vs V spectra. We show three representative tunneling spectra in Figs. 1(b)–1(d). All the spectra are normalized to the conductance at 10 mV around which the conductance remains flat. In each of these panels we also show the best

*goutam@iisermohali.ac.in

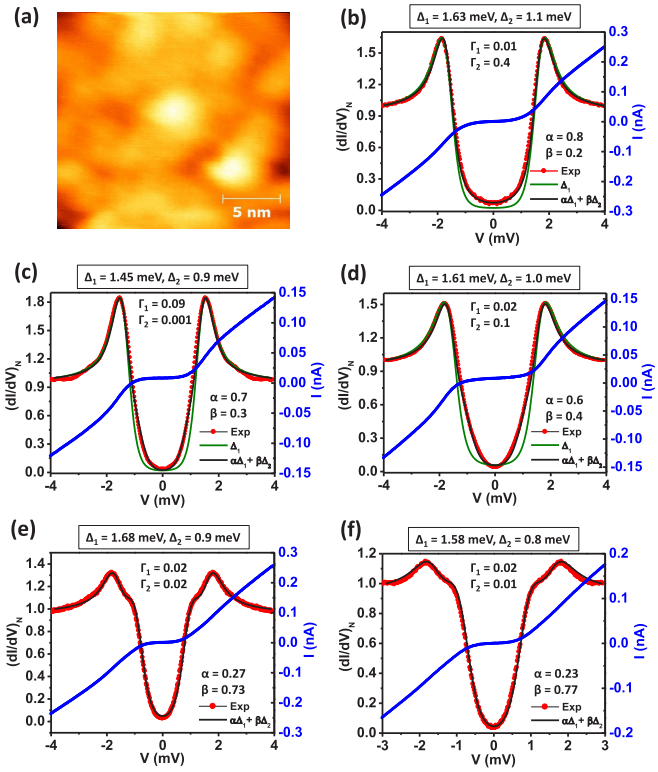

FIG. 1. (a) STM topograph image of the sample. (b)–(e) Tunneling spectra (dI/dV vs V plots) with theoretical fits using Dynes equation showing two gaps measured at 1.9 K. The color dots are experimental data, solid lines show fits with single gap (green line) and with double gap (black line).

theoretical fits (green lines), first assuming a single gap originating from a single band in the Fermi surface. For a single band superconductor, the tunneling current $I(V) \propto \int_{-\infty}^{+\infty} N_s(E)N_n(E-eV)[f(E)-f(E-eV)]dE$, where $N_s(E)$ and $N_n(E)$ are the normalized density of states of the BCS-like superconducting sample and the normal metallic tip, respectively, while $f(E)$ is the Fermi-Dirac distribution function [17]. As per Dyne's formula $N_s(E) = \mathrm{Re}(\frac{(E-i\Gamma)}{\sqrt{(E-i\Gamma)^2-\Delta^2}})$, where Γ is an effective broadening parameter included to take care of slight broadening of the BCS density of states possibly due to finite life time of quasiparticles [18]. This was used to calculate the single band $\frac{dI}{dV} = \frac{d}{dV}(G_N \int_{-\infty}^{+\infty} N_s(E)N_n(E-eV)[f(E)-f(E-eV)]dE)$, where $G_N = \frac{dI}{dV}|_{V \gg \Delta/e}$. As it is clearly seen, the best theoretical fits within a single-band model deviated significantly from the experimentally obtained spectra. We then attempted to fit the spectra within a simplistic two-band model [19,20]. If superconductivity appears in two distinct bands, then the tunneling current will have contributions from both bands. Within a simplistic two-band model, the total tunneling current $I_{\mathrm{total}} = \alpha I(V, \Delta_1, \Gamma_1) + \beta I(V, \Delta_2, \Gamma_2)$, where Δ_1 and Δ_2 are the gaps formed in the two different bands, respectively, and Γ_1 and Γ_2 are the corresponding effective broadening parameters. Γ_1 and Γ_2 also include the effective interband scattering, if any. The microscopic origin of Γ in such analysis is of not much relevance and all physical processes leading to broadening are incorporated in Γ. α and β stand for the relative contribution of the two bands to the total tunneling current. Physically, α and β could be associated with the crystal facet that the tip predominantly probes and how the crystallographic axis of a particular grain is oriented with respect to the tunneling barrier. α and β might vary significantly when the tip moves from one particular orientation of a grain to another. As it is seen, the theoretically obtained spectra within the simplistic two-band model fit remarkably well with the experimental spectra revealing the existence of two gaps with magnitude $\Delta_1 \sim 1.6$ meV and $\Delta_2 \sim 0.9$ meV, respectively.

For all three representative spectra presented in Figs. 1(b)–1(d), α remained to be significantly larger than β. This observation is similar to the STM spectra obtained on polycrystalline MgB_2 [9]. However, in case of MgB_2, for certain grains, spectral signature of the two gaps could be distinctly obtained on certain tunneling spectra recorded on appropriate grains where, due to particular orientation of the tunneling barrier with respect to the crystal plane of the grains, the smaller gap coupled more strongly than the larger gap. Motivated by this, we explored the tunneling spectra on a large number of grains and indeed for certain grains we achieved the "two-gap" feature in a given tunneling spectrum. Two such representative spectra along with two-gap fits are shown in Figs. 1(e) and 1(f), respectively. While the gap amplitude for the smaller gap and the larger gap remained approximately the same as before, for these spectra, α turned out to be smaller than β which is consistent with the understanding that the two-gap feature is seen in a single spectrum when the band corresponding to the smaller gap has a larger contribution to the tunneling current.

It should be noted that the superconducting energy gap is the manifestation of a phase-coherent macroscopic condensate and typically the gap measured by STM at the surface agrees very well with the gap amplitude that is measured by bulk-sensitive techniques like specific heat, for example. Again, Mo_8Ga_41 is metallic and no special surface states are expected which might, arguably, give rise to surface superconductivity independent of the bulk. In our case we have considered the surface very carefully and found that the two-gap superconductivity remained at all points on the surface while only the relative amplitudes varied from one point to another. In principle, it might also be imagined that proximity effect could give rise to two superconducting gaps in the system where a superconducting gap is induced in the tip giving rise to the two-gap feature in spectroscopy. However, within this hypothetical picture it is impossible to comprehend how the relative contribution of the two gaps would systematically (and reproducibly) vary from point to point. It may also be argued that owing to the extreme surface sensitivity of STM experiments, for an unclean surface, even a small layer of foreign material may acquire a proximity induced superconducting character thereby leading to the observation of two gaps. In our case, however, we have cleaned the surface under UHV conditions for 20 min by (reverse) sputtering with Ar ions in our integrated UHV preparation chamber and immediately transferred the sample to the low-temperature stage prior to the STM measurements. That is why we have been able to obtain clean spectra at all points that we have measured. Existence of a thicker layer of foreign

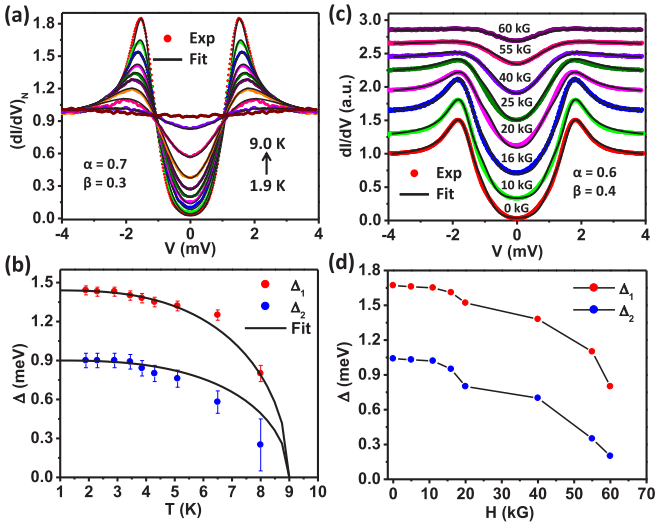

FIG. 2. (a) Temperature dependence of tunneling conductance spectra (700 mV, 250 pA) with theoretical fits. The color dots are experimental data and black lines show fits with double gap. (b) Delta vs temperature plot extracted from plot (a), the dots are values extracted from the theoretical fits and the solid line shows the temperature dependence as per BCS theory. (c) Magnetic field dependence of tunneling conductance spectra (400 mV, 250 pA) with theoretical fits. The color dots are experimental data and black lines show fits with double gap. (d) Delta vs H plot extracted from plot (c).

material would, in fact, mask the underneath gap due to the surface sensitivity of the measurements. Furthermore, the lateral proximity effect is also ruled out as both gaps are clearly resolved in a single spectrum acquired at one point. Therefore, based on the data presented above, it is rational to conclude that we have provided spectroscopic evidence of two-band superconductivity in Mo_8Ga_{41}.

To gain further understanding on the multiband superconductivity in Mo_8Ga_{41} we now focus on the magnetic field dependence of the tunneling spectra. To understand the effect of the magnetic field on the superconducting energy gap, we fit the spectra recorded at different magnetic fields using the same formula that was used for the zero-field spectra. The spectra with fitting are shown in Fig. 2(c). The extracted values of the two gaps as a function of magnetic field are shown in Fig. 2(d). The larger gap (Δ_1) decreases slowly and attains 53% of its zero field value at a magnetic field of 6 T, beyond which reasonable estimate of the gap was not possible. The smaller gap (Δ_2), on the other hand, falls rapidly with increasing magnetic field. At a field of 6 T, the gap becomes 0.15 meV which is only less than 15% of the gap at zero field. This variation of the two gaps in Mo_8Ga_{41} is similar to the variation of the two gaps with magnetic field in MgB_2, where the small gap is seen to disappear at a magnetic field of approximately 1 T, whereas the large gap remains almost unaffected within this range of magnetic field [14]. Furthermore, this observation is also consistent with the theoretical calculations of the vortex state of a multiband superconductor with weak interband scattering [21,22]. For the larger gap of Mo_8Ga_{41}, $2\Delta_1/k_BT_c$ is found to be 3.5 which is close to the expected value for a weak-coupling BCS superconductor. This suggests that the critical temperature T_c in this compound is governed by the larger gap (Δ_1). This again is similar to MgB_2 and YNi_2B_2C, where multiband scattering is weak [23] and is again consistent with the theoretical expectation for a multiband superconductor with weak interband scattering [21,22]. Therefore, from our field dependent study of the superconducting energy gaps we surmise that the interband scattering in Mo_8Ga_{41} is weak and falls in a range similar to that in MgB_2. That might also explain why the qualitative spectral features in Mo_8Ga_{41} are remarkably similar to those in MgB_2.

Our observation of weak coupling superconductivity in Mo_8Ga_{41} differs from the strong coupling superconducting behavior that was reported based on μSR and specific heat measurements [7,8]. Unlike these techniques, our conclusion is based on direct spectroscopic measurements of the superconducting energy gaps. However, our most important conclusion, i.e., multiband superconductivity, is consistent with the conclusions drawn from the μSR and specific heat measurements [7,8].

Now we focus on the nature of the two gaps of Mo_8Ga_{41}. In Fig. 2(a) we show the temperature dependence of one representative spectrum over a temperature range from 1.9 to 9 K. The colored dots represent the experimentally obtained spectra. The coherence peaks gradually decrease with increasing temperature and the features associated with superconductivity disappear above 9 K. In the same panel we also show the fits within the two-band model discussed above. For the entire temperature range, the values of α and β remained fixed. The two gaps extracted (red and blue dots) are plotted with temperature in Fig. 2(b). The black lines show the expected temperature dependence as per BCS theory [17] for the two individual gaps with same T_c. As it is seen, the larger gap (Δ_1) follows BCS temperature dependence. The smaller gap, on the other hand, remains constant up to almost 4 K and then starts gradually dropping and disappearing at 9 K showing only slight deviation from the BCS prediction [17]. The disappearance of both gaps at approximately the same temperature excludes the possibility of stoichiometric disorder in the grains on the sample.

In order to understand the origin of exotic multiband superconductivity in Mo_8Ga_{41}, we investigated the band structure of the system through first-principles electronic structure calculations. The calculations are performed within the framework of density functional theory (DFT) [24,25] using generalized gradient approximation (GGA) [26] of the Perdew-Burke-Ernzerhof (PBE) [26] form for the exchange-correlation functional as implemented in the Vienna *ab initio* simulation package (VASP). The projector augmented wave (PAW) [27] pseudopotentials are used to describe the core electrons. Electronic wave functions are expanded using plane waves up to a cut-off energy of 500 eV. The Monkhorst-Pack k mesh is set to $6 \times 6 \times 6$ in the Brillouin zone for the self-consistent calculation. All atoms are relaxed in each optimization cycle until atomic forces on each atom are smaller than 0.01 eV/Å.

Mo_8Ga_{41} belongs to the space group of $R\bar{3}$ (No. 148) with a rhombohedral structure [2]. We obtained the relaxed lattice parameters as $a = b = c = 9.5788$ Å, which are close to the experimental values, and $\alpha = \beta = \gamma = 94.974^\circ$ [2]. Each Mo atom is surrounded by ten Ga atoms, forming a polyhedron

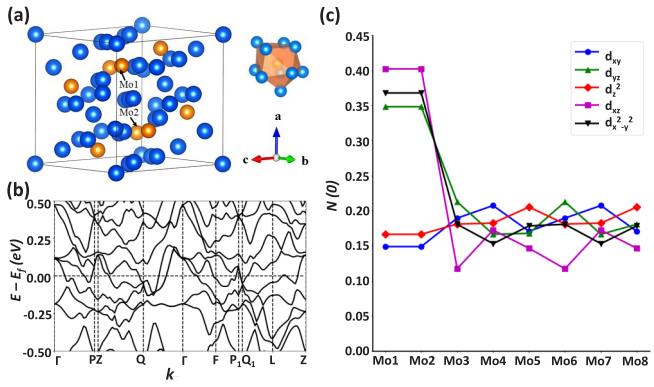

FIG. 3. (a) Crystal structure of Mo_8Ga_{41}. (b) Computed band structure plotted along the high-symmetric directions. (c) Computed total density of states at the Fermi level for different Mo sites and different d orbitals. The site selectivity is clearly observed.

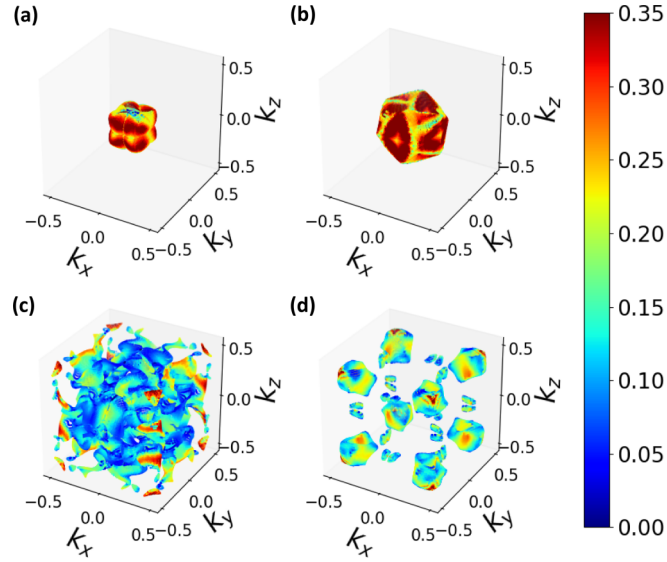

FIG. 4. 3D Fermi surfaces (pockets) with Fermi velocities shown as color maps on the pockets.

as shown in the Fig. 3(a) [3]. We discuss below that despite having the similar polyhedron nest around all eight Mo atoms, two of them have stronger contributions to the Fermi surfaces. This is the primary origin of the site-selective superconductivity in this compound. To deal with the strong correlation effect of the d electrons of the Mo atoms, we employed the GGA+U method with $U = 4$ eV.

In Fig. 3 we show one of our main theoretical findings. We evaluated site and orbital resolved density of states $N_\sigma(0)$ at the Fermi level, and compared them in Fig. 3(c). We notice that only Mo1 and Mo2 sites as shown in Fig. 3(a) contribute strongly to the Fermi surface. Among all the d orbitals of the Mo atoms, d_{xz}/d_{yz} and $d_{x^2-y^2}$ orbitals have the strongest contributions, while the other orbitals and Mo atoms have significantly less contributions to the low-energy states.

In Fig. 3(b) we show the band dispersion of the paramagnetic phase along the high-symmetric momenta directions. In order to identify the relation of the electronic structure with the observed multiple superconducting gaps, we now focus on the low-energy regime. We notice that there are four bands passing through the Fermi level with considerable three dimensionality in all of them. Three-dimensional (3D) views of the corresponding Fermi surfaces are shown in Fig. 4 with Fermi velocities plotted as a color map. We find two concentric hole pockets around the Γ point, and one tiny electron pocket around the Brillouin zone corner. In addition, we also find a large and strongly anisotropic Fermi surface all over the Brillouin zone, a typical feature in this materials class. Within the BCS theory, superconducting order parameter is defined in the band basis in the **k** space. Earlier, in MgB_2, a two-band superconductivity was reported where the interband electron-phonon coupling was found to play an important role [9,10]. In a superconducting iron-pnictide family, a multiband Fermi surface topology also leads to observation of multiple superconducting gaps [28]. By projecting the orbital weights of iron atoms onto the Fermi surface topology, recent reports found an exotic orbital selective characteristic in the superconducting order parameter. This orbital selective behavior provided important clues to the orbital fluctuations (or entangled spin-orbital fluctuation owing to strong Hund's coupling in iron-pnictides) mediated superconducting pairing interaction. On the same footing, our observation of site-selective behavior on the low-energy electronic structure paves the way for a new mechanism of site-fluctuations induced pairing interaction responsible for superconductivity in Mo_8Ga_{41}.

Having shown the evidence of multiband superconductivity in Mo_8Ga_{41}, we now attempt to identify the bands that might be responsible for the smaller and the larger superconducting gaps, respectively. In order to identify that, we have calculated the effective Fermi velocities in different bands. The distribution of the Fermi velocity is shown as color maps on the four Fermi sheets as shown in Fig. 4. It is found that the average velocity on the two pockets around the Γ point is significantly larger than that around the other pockets. From qualitative understanding of phonon mediated pairing, it can be rationalized that for two distinct bands taking part in superconductivity, when the average Fermi velocity in a band is significantly larger than that in the other band, the superconducting gap forming on the band with higher average Fermi velocity should be lower than that forming in the other band. This is nothing but the manifestation of the semiclassical idea that it is harder for the faster electrons to interact strongly with the lattice as it spends less time near a given lattice point. On the other hand, slower electrons spend longer duration passing a given lattice points thereby leading to a larger electron-phonon coupling. This causes the band with relatively slower electrons form a stronger superconducting energy gap. A similar observation was made in case of the multiband superconductor YNi_2B_2C [23]. Therefore, based on our data and theoretical analysis, we can conclude that the smaller gap forms in the bands shown in Fig. 4(a) or 4(b) while the larger gap forms in the bands shown in Fig. 4(c) or 4(d). It is also noticed that the Mo1 and Mo2 sites have approximately similar contribution to the DOS at the Fermi level. Therefore, it is rational to conclude that the difference in the superconducting gap is rising due to the difference in the Fermi velocities. Additional experiments like quantum

oscillations in the superconducting state may provide information on the exact bands that participate in superconductivity. That might help identify the bands responsible for the two gaps with more precision.

In conclusion, we have provided direct spectroscopic evidence of multiband superconductivity in the endohedral gallide Mo_8Ga_{41} through detailed temperature and magnetic field dependent scanning tunneling spectroscopy and through band structure calculations. Analysis of the temperature dependent spectra within a two-gap BCS model revealed that both gaps follow BCS temperature dependence. From a qualitative analysis of the magnetic field dependent STS spectra we surmise that in terms of the strength of interband scattering, Mo_8Ga_{41} falls in the same range as MgB_2. Our band structure calculations revealed a unique site-selective mechanism that facilitates the observed multiband superconductivity in Mo_8Ga_{41}.

G.S. would like to acknowledge financial support from the research grant of Swarnajayanti fellowship awarded by the Department of Science and Technology (DST), Govt. of India under the Grant No. DST/SJF/PSA-01/2015-16. S.P. acknowledges the SERB for support through Grant No. EMR/2016/003998.

[1] B. Matthias, Phys. Rev. **97**, 74 (1995).
[2] A. Bezinge, K. Yvon, M. Decroux, and J. Muller, J. Less-Common Met. **99**, L27 (1984).
[3] W. Xie, H. Luo, B. F. Phelan, T. Klimczuk, F. A. Cevallos, and R. J. Cava, Proc. Natl. Acad. Sci. USA **112**, E7048 (2015).
[4] E. D. Bauer, M. M. Altarawneh, P. H. Tobash, K. Gofryk, O. E. Ayala-Valenzuela, J. N. Mitchell, R. D. McDonald, C. H. Mielke, F. Ronning, and J.-C. Griveau, J. Phys.: Condens. Matter **24**, 052206 (2012).
[5] N. J. Curro, T. Caldwell, E. D. Bauer, L. A. Morales, M. J. Graf, Y. Bang, A. V. Balatsky, J. D. Thompson, and J. L. Sarrao, Nature (London) **434**, 622 (2005).
[6] D. Daghero, M. Tortello, G. A. Ummarino, J.-C. Griveau, E. Colineau, R. Eloirdi, A. B. Shick, J. Kolorenc, A. I. Lichtenstein, and R. Caciuffo, Nat. Commun. **3**, 786 (2012).
[7] V. Yu. Verchenko, A. A. Tsirlin, A. O. Zubtsovskiy, and A. V. Shevelkov, Phys. Rev. B **93**, 064501 (2016).
[8] V. Yu. Verchenko, R. Khasanov, Z. Guguchia, A. A. Tsirlin, and A. V. Shevelkov, Phys. Rev. B **96**, 134504 (2017).
[9] J. A. Silva-Guillén, Y. Noat, T. Cren, W. Sacks, E. Canadell, and P. Ordejon, Phys. Rev. B **92**, 064514 (2015).
[10] M. Iavarone, G. Karapetrov, A. E. Koshelev, W. K. Kwok, G. W. Crabtree, D. G. Hinks, W. N. Kang, E.-M. Choi, H. J. Kim, H.-J. Kim *et al.*, Phys. Rev. Lett. **89**, 187002 (2002).
[11] F. Giubileo, D. Roditchev, W. Sacks, R. Lamy, D. X. Thanh, J. Klein, S. Miraglia, D. Fruchart, J. Marcus, and P. Monod, Phys. Rev. Lett. **87**, 177008 (2001).
[12] H. Schmidt, J. F. Zasadzinski, K. E. Gray, and D. G. Hinks, Phys. Rev. Lett. **88**, 127002 (2002).
[13] P. Szabó, P. Samuely, J. Kačmarčík, T. Klein, J. Marcus, D. Fruchart, S. Miraglia, C. Marcenat, and A. G. M. Jansen, Phys. Rev. Lett. **87**, 137005 (2001).
[14] R. S. Gonnelli, D. Daghero, G. A. Ummarino, V. A. Stepanov, J. Jun, S. M. Kazakov, and J. Karpinski, Phys. Rev. Lett. **89**, 247004 (2002).
[15] F. Bouquet, R. A. Fisher, N. E. Phillips, D. G. Hinks, and J. D. Jorgensen, Phys. Rev. Lett. **87**, 047001 (2001).
[16] X. K. Chen, M. J. Konstantinović, J. C. Irwin, D. D. Lawrie, and J. P. Franck, Phys. Rev. Lett. **87**, 157002 (2001).
[17] J. Bardeen, L. N. Cooper, and J. R. Schrieffer, Phys. Rev. **108**, 1175 (1957).
[18] R. C. Dynes, V. Narayanamurti, and J. P. Garno, Phys. Rev. Lett. **41**, 1509 (1978).
[19] H. Suhl, B. T. Matthias, and L. R. Walker, Phys. Rev. Lett. **3**, 552 (1959).
[20] E. J. Nicol and J. P. Carbotte, Phys. Rev. B **71**, 054501 (2005).
[21] A. E. Koshelev and A. A. Golubov, Phys. Rev. Lett. **90**, 177002 (2003).
[22] N. Nakai, M. Ichioka, and K. Machida, J. Phys. Soc. Jpn. **71**, 23 (2002).
[23] S. Mukhopadhyay, G. Sheet, P. Raychaudhuri, and H. Takeya, Phys. Rev. B **72**, 014545 (2005).
[24] P. Hohenberg and W. Kohn, Phys. Rev. **136**, B864 (1964).
[25] W. Kohn and L. J. Sham, Phys. Rev. **140**, A1133 (1965).
[26] J. P. Perdew, K. Burke, and M. Ernzerhof, Phys. Rev. Lett. **77**, 3865 (1996).
[27] P. E. Blöchl, Phys. Rev. B **50**, 17953 (1994).
[28] R. Yu and Q. Si, Phys. Rev. B **96**, 125110 (2017).